Inverse pion photoproduction in the vicinity of the $P_{33}(1232)$ resonance and a test of time-reversal invariance*

J. C. Comiso,† D. J. Blasberg,‡ R. P. Haddock, B. M. K. Nefkens, P. Truoel,§ and L. J. Verhey
Physics Department, University of California, Los Angeles, California 90024
(Received 18 December 1974)

Differential cross-section measurements are presented for $\pi^- p \to \gamma n$ at five energies around the $P_{33}(1232)$ resonance. A detailed comparison is made with $\gamma n \to \pi^- p$ deduced from γd experiments. In general, the results are in support of detailed balance. Using the Christ-Lee–Donnachie-Shaw model, our new data indicate that the T-violating phase in the isovector part of the M_{1+} multipole is less than 2°, which is a very sensitive test of time-reversal invariance. No evidence is found for a possible isotensor component of the electromagnetic current. Our data are compared to various multipole analyses. In general, the agreement is poor.

I. INTRODUCTION

The reasons for studying REX (radiative exchange) or inverse pion photoproduction,

$$\pi^- + p \to \gamma + n\,, \tag{1}$$

have been discussed in detail in our previous article[1] on the subject. The most exciting aspect is a test of time-reversal invariance of the electromagnetic interactions of hadrons[2] through a comparison of the REX cross section with its inverse. The experiment reported here covers five energies in the vicinity of the $P_{33}(1232)$ πN resonance. The comparison error which is defined in Ref. 1 and which limited the sensitivity of our first measurement somewhat is substantially reduced here. Otherwise, the experiment is similar to the earlier one except that it covers the region between $\tilde{E} = 1191$ MeV and $\tilde{E} = 1285$ MeV (the tilde denotes a center-of-mass variable).

II. EXPERIMENTAL ARRANGEMENT

The experiment was performed at the 184-in. cyclotron of the Lawrence Berkeley Laboratory. The detection apparatus, shown in Fig. 1, consisted of 4 beam hodoscope planes H_α, H_β, H_γ, H_δ and a timing counter T to define the incident beam direction; 6 anticounters $\bar{A}_{S1} - \bar{A}_{S5}$ and $\bar{A}_H$ surrounding the target to enhance triggering on neutral final-state particles; a 76×76 cm, heavy plate, 40-gap, optical spark chamber interspersed with scintillation counters to detect the photons; and a semi-close-packed set of 32 carefully calibrated[3] neutron counters for good spatial resolution, each counter with its own zero-crossing discriminator to optimize time-of-flight (TOF) measurements. This equipment is described in detail in Refs. 1, 4, and 5. The only significant change made in the original setup was the removal of the π^0 anticounters, which had proven to be of little use in the event determination and were mainly used to reduce the triggering rate. The electronics, triggering mode, and data analysis have already been detailed,[1,4,5] and we restrict ourselves to a short description of the five new pion beams.[5] The negative pions were produced on an internal beryllium target. The beam transport system was of the intermediate focus type. It consisted of the cyclotron fringe field, two sets of quadrupole magnets, two bending magnets, and a long collimator. The final beam focus was in the experimental area in the hydrogen target. The properties of the five pion beams are given in Table I. The beam momentum was determined in two ways. Firstly, we used range measurements in copper. A correction for multiple scattering of 2.7–2.9% was applied to the measured range and we used the range-energy tables of Ref. 6. We also determined the incident beam momentum from the $n\gamma$ opening angle of a selected sample of REX events at every data point. The agreement with the range curve is very good, as indicated in Table II. The final value used is an average of both methods. The momentum spread of the incident beam was deduced from the range curve, and it agreed with the analysis of the $n\gamma$ opening angle of charge-exchange events (CEX) recorded with the same equipment. This is discussed in detail in Ref. 5. The beam contamination was arrived at in the following way. The electron contamination was investigated with a Freon-gas Cerenkov counter, calibrated in a previous experiment. Unfortunately, the efficiency was not rechecked after our experiment, and we suspect that the efficiency may not have remained constant during the experiment, necessitating the assignment of a substantial error. The off-momentum muons, $p_\mu \neq p_\pi$, from pion decay in the downstream section of the beam, were calculated with a Monte Carlo program that used the measured spatial

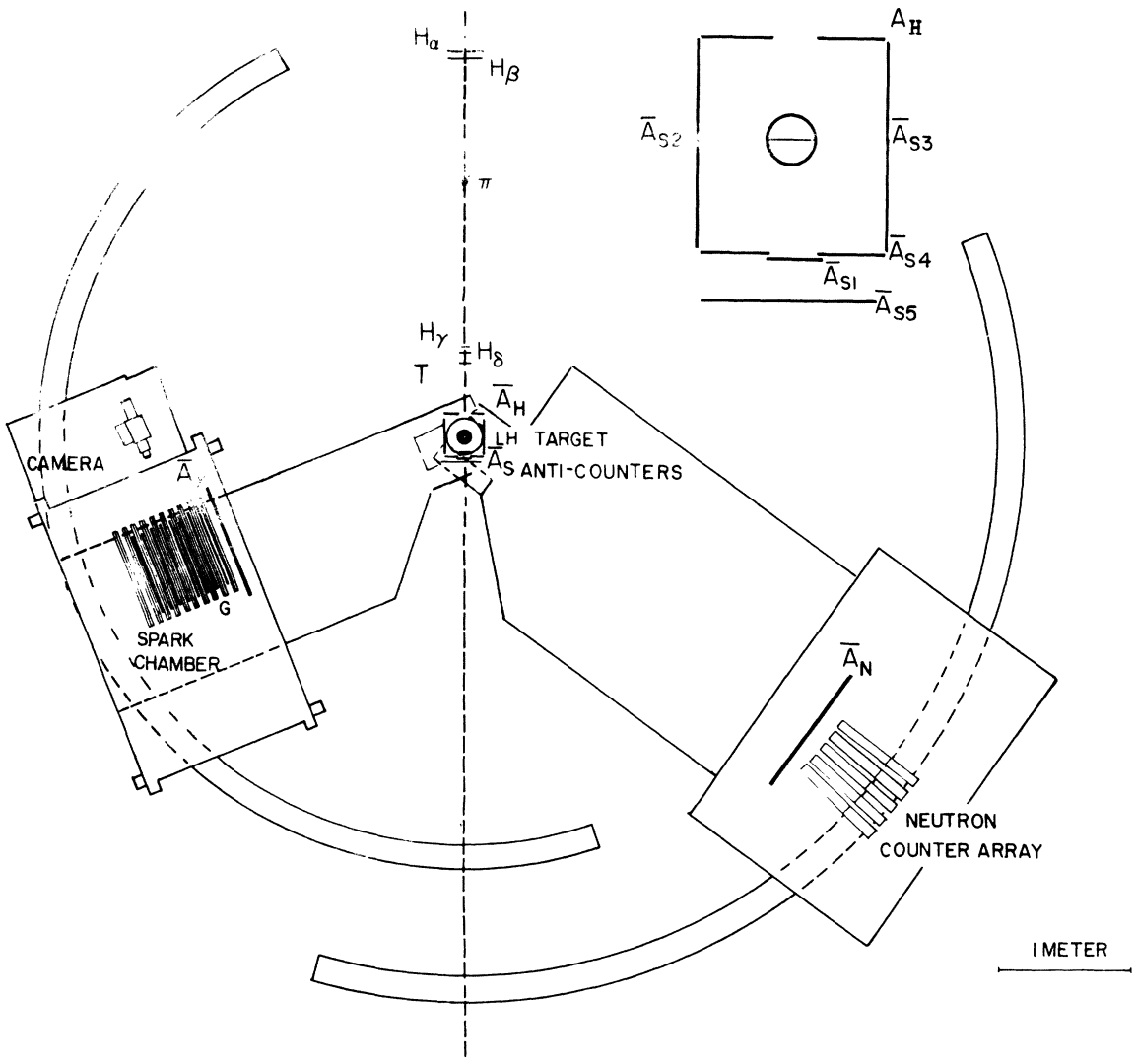

FIG. 1. Experimental setup. The anticounters around the hydrogen target are shown separately on the top right.

and momentum distributions of the beam as input data. The on-momentum muons, $p_\mu = p_\pi$, were extracted from the range curve. As an over-all check on our beam contamination and beam energy, we compared the CEX results extracted from our data with phase-shift predictions. The agreement is good, as detailed in the subsequent paper.[7] Furthermore, the fraction of pions that disappeared in the hydrogen target, the so-called π_{stop} of Ref. 1, was recorded routinely through the ex-

TABLE I. Properties of the pion beams.

Beam	c.m. energy $\tilde{E}$ (MeV)	Peak lab. mom. (MeV/c)	Mom. spread $\pm\Delta p/p$	Rate ($10^6\,\pi^-$/sec)	e^-	Contamination in % $p_\mu - = p_\pi$	$p_\mu - \neq p_\pi$	Total
1	1191 ± 2	239 ± 3	5.9%	1.2–1.8	5.6	6.0	9.8	21.4 ± 3.6
2	1208 ± 2	264 ± 3	4.5	0.9–1.2	2.1	4.3	9.9	16.3 ± 2.6
3	1230 ± 2	295 ± 3	5.8	0.7–0.8	2.3	4.9	9.8	17.0 ± 3.0
4	1249 ± 2	323 ± 3	3.7	1.1–1.3	3.6	2.9	9.2	15.7 ± 2.2
5	1285 ± 3	375 ± 4	4.0	1.2–1.4	0.8	2.6	7.9	11.3 ± 1.7

periment, and was used to obtain $\sigma_t(\pi^- p \to \text{neutrals})$. The comparison of this σ_t with the published measurements[8] gave a check of about 12% on the beam contamination.

III. DATA PROCESSING

The film, data selection, event parameterization, event reconstruction, Monte Carlo simulations, and fitting procedures have all been discussed extensively.[1,4,5] To extract the events from the background, we made us of three parameters: (1) the measured neutron time of flight τ_x; (2) the deviation from coplanarity D_n of the neutron, gamma, and incident π^-; (3) the π^- momentum p_x evaluated from the $n\gamma$ opening angle. We first calculated the difference between the measured values τ_x, D_n, p_x and the expected values τ_k, 0, p_k. Next we normalized these numbers by dividing each difference by its expected uncertainty σ due to the finite target size, beam divergence, and detector resolution; thus

$$S_\tau = (\tau_k - \tau_x)/\sigma_\tau , \tag{2a}$$

$$S_p = (p_k - p_x)/\sigma_p , \tag{2b}$$

$$S_D = D_n/\sigma_D . \tag{2c}$$

We then calculated "pseudo-χ^2" values for each event from these three parameters:

$$\chi^2(p_k, \tau_k) = S_p^2 + S_\tau^2 , \tag{3a}$$

$$\chi^2(p_k, D_n) = S_p^2 + S_D^2 , \tag{3b}$$

$$\chi^2(\tau_k, D_n) = S_\tau^2 + S_D^2 , \tag{3c}$$

and

$$\chi^2(p_k, \tau_k, D_n) = S_p^2 + S_\tau^2 + S_D^2 . \tag{4}$$

Thus, for every data point, we calculated four frequency distributions of "pseudo-χ^2" values.

The event extraction was based on the comparison of the four χ^2 distributions of Eqs. (3) and (4) of our data with those of the Monte Carlo generated events. Typically 90% of the REX events have a pseudo $\chi^2 < 3$. The rest have undergone a scattering which results in a larger value, but rarely exceeding 5. On the other hand, CEX and random events have a pseudo-χ^2 value anywhere between 0 and a large number (frequently exceeding 500). Now, events with a large χ^2 have no relation to the REX events and reduce the significance of the χ^2 per degree of freedom that is used to express the comparison of data with Monte Carlo. Thus, the comparison of the pseudo-χ^2 distributions was usually restricted to the χ^2 region below $\chi^2 = H$, where the value of H was chosen to be 20, 30, 40, or 50. The number of REX events, N_{REX}, must be independent of the choice for H and we very carefully checked this aspect for all pseudo-χ^2 distributions for every data point. As a final note, we remark that the χ^2 distributions of Eq. (3) can be improved by applying a cut on the unused third parameter, say, 2.5 standard deviations. Again, N_{REX} should be independent of the cut. The value of N_{REX} used in the calculation of the cross section is the one from the distribution that has "stable" results despite extreme cuts and the smallest error. The pseudo χ^2 based on coplanarity and beam momentum with a 2.5-standard-deviation cut on the neutron time of flight and the χ^2-region $\chi^2 < 40$ was used most frequently.

TABLE II. Comparison of the beam momentum as determined from range measurements and from $n\gamma$ opening angle of selected REX events.

Beam	Momentum in MeV/c	
	Range method	$n\gamma$ angle, REX
1	240 ± 3	239 ± 3
2	264 ± 3	264 ± 3
3	295 ± 3	295 ± 3
4	324 ± 3	323 ± 3
5	374 ± 4	375 ± 3

The event extraction procedure outlined above will now be illustrated; the example used is our measurement at $\bar{E} = 1285$ MeV and $\bar{\theta}_\gamma = 88°$. The distributions of the values for τ_x, D_n, and p_x for this data point are shown in Fig. 2. The solid line is the experimental data corrected for the result of target empty runs, and the dashed line is the Monte Carlo generated background of CEX and random events. At the angle chosen for illustration, the difference in neutron TOF between CEX and REX is a few nsec. The small amount of REX can be found on top of the high CEX peak in Fig. 2(a) centered around $\tau_x = 31.3$ nsec and could never be isolated reliably by TOF technique only. But the REX events do produce a better peak in the coplanarity distribution, Fig. 2(b), centered around 0. Also, the reconstructed beam momentum, which is derived from the measured $n\gamma$ opening angle, shows a REX peak, though a broad one, centered around 375 MeV/c above the flat CEX background. In Fig. 3 is shown how the simultaneous use of two of the above three parameters in the manner given by Eq. (3), plus a cut in the third parameter, leads to a useful separation of REX from background, and Fig. 4 shows the results of applying all three parameters simultaneously. The pseudo-χ^2 distributions extend to $\chi^2 = 25$; thus $H = 25$ in the above notation. In all three cases, Fig. 3(a)–3(c), one sees a nice peak

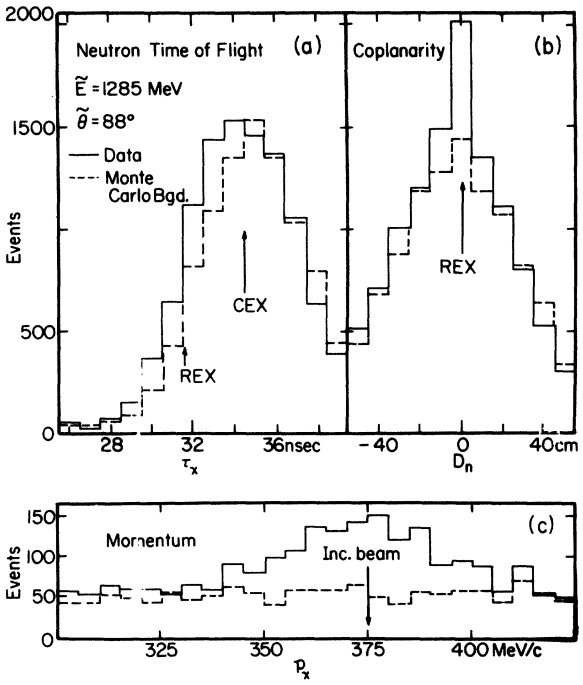

FIG. 2. Example of a comparison between our data, given by the solid line, and the Monte Carlo simulation of charge exchange and random background, shown by the dashed line. The difference between the two distributions is due to REX. (a) Neutron time-of-flight spectrum. (b) Coplanarity as defined in Ref. 1. (c) Reconstructed incident beam momentum deduced from the measured $n\gamma$ opening angle.

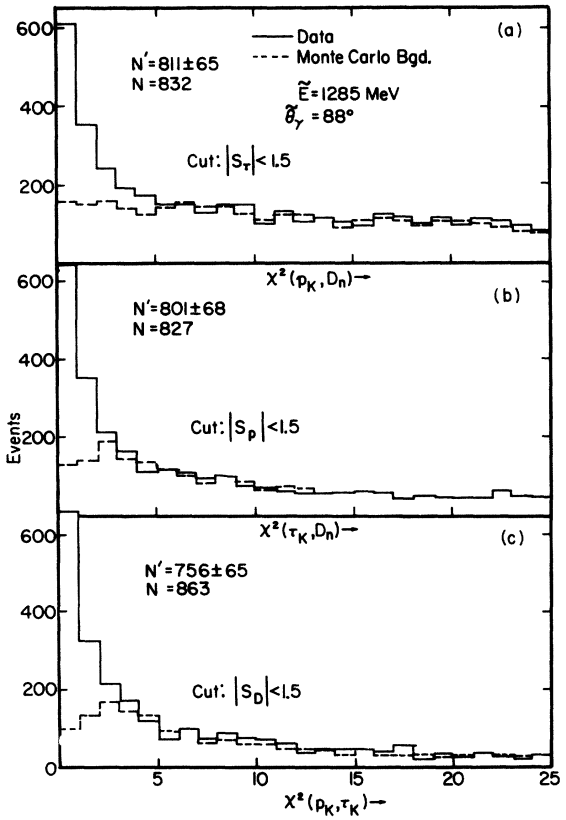

FIG. 3. The three pseudo-χ^2 distributions of Eq. (3) for a representative data point. N' = number of events extracted. N = total number of events corrected for the events lost due to the indicated cut in the third variable.

at low χ^2 which has the expected shape of REX plus background. The number N' given in each figure is the number of REX events determined from the χ^2 distribution plotted. The real number of REX events N is obtained from N' by applying a correction calculated by Monte Carlo technique for events lost because of the cut. The agreement in the values for N of the four different extractions given in Figs. 3 and 4 is very gratifying. In Figs. 5(a) and 5(b) we have shown a representative sample of distributions of $\chi^2(p_k, D_n)$ with a cut $|S_\tau| < 2.5$ or 3.5. The resolution of the experiment is everywhere sufficient for the separation of REX from the large background.

Our data points with $\tilde{\theta}_\gamma \lesssim 60°$ are special in the sense that the neutron time-of-flight separation for REX and CEX is sufficiently large to attempt to determine N_{REX} in the manner used by the Lausanne-Munich collaboration using TOF only.[9] All events that have the expected REX neutron TOF are tested for coplanarity. The noncoplanar event distribution is used for the background subtraction, the shape of which must be calculated with a Monte Carlo program. The number of events thus obtained agrees with the more elaborate method discussed above.

IV. CALCULATION OF CROSS SECTIONS

The center-of-mass $\pi^- p \to \gamma n$ cross section was obtained from the expression

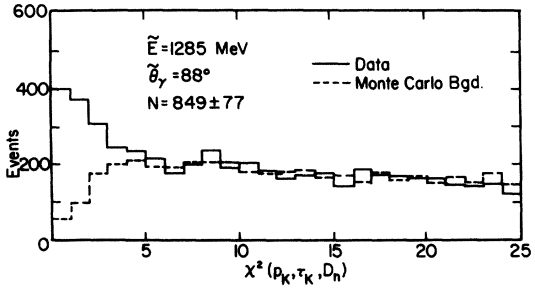

FIG. 4. Pseudo-χ^2 distribution of Eq. (4) for same data point as Fig. 3.

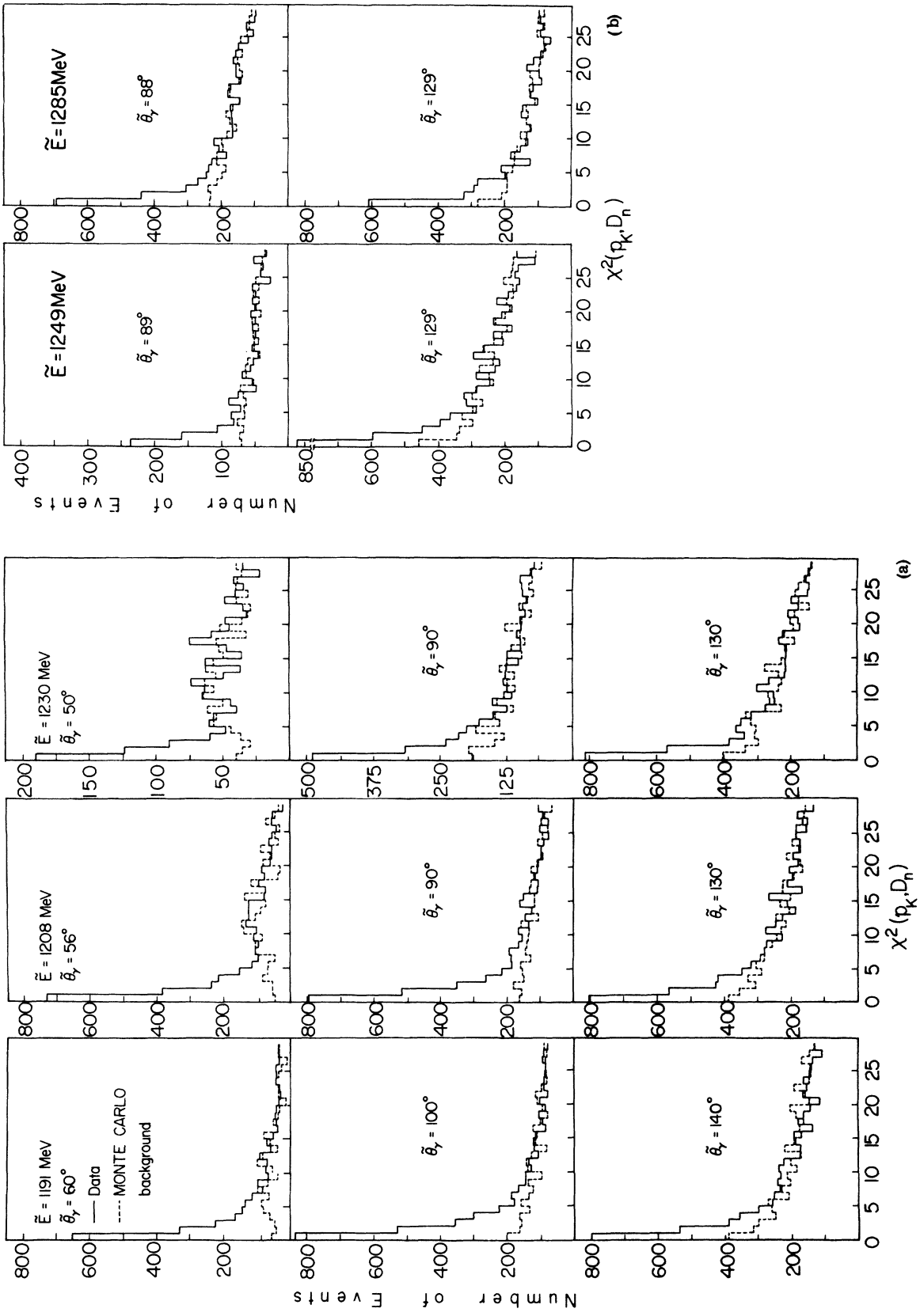

FIG. 5. (a) Representative examples of pseudo-$\chi^2(p_k, D_n)$ distribution with a cut $|S_T|<2.5$, at one forward, center, and backward angle of our data. The solid solid line is our experimental data. The dashed line is the Monte Carlo generated background of CEX and random events. (b) Same as (a), but with a cut $|S_T|<3.5$, at one center and backward angle.

$$d\sigma/d\tilde{\Omega} = N_{\mathrm{REX}}/\pi_{\mathrm{in}} Jf . \quad (5)$$

N_{REX} is the number of REX events minus the number of empty-target REX events; π_{in} is the number of incident pions; J is the Jacobian of the neutron detector; and f is the product of all other cross section factors such as the neutron- and photon-counter efficiencies, the effective target thickness, solid angle, and eight correction factors listed in Ref. 1. The nontrivial correction factors concern the beam doubles, the beam contamination, malfunctioning of the neutron TOF system that caused some REX and CEX neutrons to appear in the TOF underflow, neutrons scattered in the hydrogen target and surrounding anticounters, and neutrons that scattered in the neutron counters without the recoil triggering the discriminator. Listed in Table III are the "direct" results of our experiment on $\pi^- p \to \gamma n$ converted for convenience to $\gamma n \to \pi^- p$ differential cross sections using the detailed-balance relation. Also listed are the number of REX events observed at each point. We have lumped together the results of all 32 neutron counters. The limited statistics and proximity of the counters to one another do not warrant an individual counter presentation.

The total error in our results can be divided into a normalization error and a relative error. Both are listed in Table III. The normalization error scales the measurements at each incident beam momentum in the same way. It is due, for example, to the uncertainties in the beam contamination. The relative error varies for each measurement. It is due, for example, to the counting statistics. The error quoted for our differential cross section measurements is obtained by combining the relative and normalization error in quadrature.

The result of our experiment can also be expressed in the form of the ratio

$$P = d\sigma(\pi^- p \to \pi^0 n)/d\sigma(\pi^- p \to \gamma n) \quad (6)$$

for a fixed neutron angle in the laboratory. This ratio is akin to the Panofsky ratio for stopped π^-'s. Listed in Table IV are our measured P = CEX/REX ratios. The error in this ratio is smaller than in the direct REX result because the ratio is insensitive to the errors in the beam contamination, neutron-counter efficiency, and automatic film scanning. Listed also in this table are the CEX values from the most recent CERN phase-shift analysis,[10] interpolated to our energies and angles, and our "indirect" REX results obtained by dividing the CERN CEX data by P and the detailed-balance factor. The error quoted for the indirect results is the one due to the error in the CEX/REX ratio and does not contain the contribution due to the error in the CEX values. The agreement of the "direct" REX results with the "indirect" REX result is good even without including the error in the CEX.

TABLE III. "Direct" results of our experiment on $\pi^- p \to \gamma n$ converted for convenience to $\gamma n \to \pi^- p$ using detailed balance. In the first column are listed the incident beam momentum in MeV/c and $\tilde{\theta}_\gamma$ in degrees for each data point.

Data point p_π-$\tilde{\theta}_\gamma$	N_{REX}	$\frac{d\sigma}{d\tilde{\Omega}}(\gamma n \to \pi^- p)$ (μb/sr)	Error (%) rel.	norm.
239-60	1559 ± 115	13.7 ± 1.5	8.7	6.3
239-80	2271 ± 353	17.9 ± 1.6	7.3	
239-100	1735 ± 154	20.5 ± 2.3	9.6	
239-120	1279 ± 108	21.4 ± 2.4	9.4	
239-140	938 ± 106	20.7 ± 2.8	12.1	
264-56	1659 ± 115	16.4 ± 1.6	8.3	5.6
264-70	1981 ± 135	22.1 ± 2.1	7.9	
264-90	1719 ± 131	28.1 ± 2.8	8.5	
264-110	1103 ± 136	28.0 ± 3.9	12.9	
264-130	1129 ± 146	24.9 ± 3.6	13.5	
264-142	1446 ± 202	29.3 ± 4.6	14.6	
295-50	758 ± 104	14.6 ± 2.2	14.5	5.2
295-70	434 ± 54	15.0 ± 2.1	13.1	
295-90	849 ± 114	18.9 ± 2.8	13.9	
295-110	997 ± 113	22.9 ± 3.0	12.0	
295-130	1202 ± 194	22.8 ± 4.0	16.6	
295-148	620 ± 106	18.2 ± 3.3	17.7	
323-69	925 ± 124	14.6 ± 2.1	14.0	4.3
323-89	377 ± 55	15.2 ± 2.4	15.1	
323-109	600 ± 76	17.3 ± 2.4	13.4	
323-129	1143 ± 183	14.6 ± 2.5	16.5	
323-146	719 ± 104	18.0 ± 2.8	15.0	
375-49	1178 ± 127	13.8 ± 1.9	11.7	7.1
375-69	660 ± 72	11.3 ± 1.5	11.5	
375-88	843 ± 67	11.9 ± 1.3	8.7	
375-108	841 ± 71	10.5 ± 1.2	9.5	
375-129	582 ± 97	10.3 ± 1.9	17.2	
375-147	703 ± 76	11.5 ± 1.6	11.7	

Two new phase-shift analyses have appeared recently. The work by Carter *et al.*[10] covers only the region of the $P_{33}(1232)$. The Saclay 1974 results[10] are the most recent ones, but they are given at a few energies only which makes interpolation to the energies of this experiment somewhat uncertain. The CERN CEX predictions agree within a few percent with the ones of the two new analyses in the energy region of this experiment.

In the subsequent paper[7] we evaluate $d\sigma(\pi^- p \to \pi^0 n)/d\Omega$ from our data and compare it to published CEX results. The comparison is very favorable.

The direct and indirect REX results are plagued by uncertainties of different origin. The direct REX results suffer from the errors in the beam contamination, counter efficiencies, and film scanning, detailed in Ref. 1. The indirect REX results suffer from the uncertainties in the CEX values, which we estimate[10] to be 7% at present, leading to comparable size errors in our direct and indirect REX results. Future improved CEX values can decrease the error in our indirect REX. We consider that the numerical average of the direct and indirect REX values represent the best REX results of our experiment and they are used in the next chapter to test various models. The averaged results are given in Table V. The error quoted is the one of the direct REX. The results described here are the final results of our experiment and replace all preliminary results contributed to conferences and meetings.

V. DISCUSSION OF RESULTS

A. Comparison with data from the inverse reaction and a test of time-reversal invariance

We can compare our data with photoproduction measurements to test time-reversal invariance via detailed balance. As we have discussed in our previous paper,[1] this test is made difficult by the uncertainty introduced in the extraction of the $\gamma n \to \pi p$ cross sections from the measured $\gamma d \to \pi^- pp$ cross sections. Little new data have become available since the time of our first experiment. Some groups have reported a reanalysis of their data at the Bonn conference. These data are used here instead of the older published ones. We list the various photoproduction experiments used.

(1) *Two counter experiments, one performed at Bonn*[11] *and the other at Tokyo.*[12] The π^+ and π^- from a deuterium target were measured under identical kinematical conditions. The π^+/π^- ratio multiplied by the $\gamma p \to \pi^+ n$ cross section[13,14] gives the $\gamma n \to \pi^- p$ cross section. Both experiments used a bremsstrahlung photon beam and suffer from the systematic 6–10% difference in the π^+ photoproduction cross sections,[13,14] negating the high statistical accuracy of the ratio measurements.

(2) *Two bubble-chamber experiments on* $\gamma d \to \pi^- pp$. The ABHHM collaboration[15] at DESY published their final results together with a discussion of corrections made to the raw data. There is no updated version of the PRFN collaboration[16] at Frascati. The ABHHM results in our energy region are some 15% higher than the PRFN data.

(3) *For the first time measurements with a monoenergetic, "tagged" photon beam have become available.*[17] The π^- and one photon were observed in coincidence, close to the free-neutron kinematics. Though these data are of poor statistical accuracy, they reveal what the authors term an "irreducible discrepancy" with the ratio data in the backward direction for the π^-. The coincidence data are lower in the backward direction; a similar behavior appears in the PRFN data.

Figure 6 displays all presently available differential cross sections derived from γd experiments for $\gamma n \to \pi^- p$ at our energies together with our results for the inverse and the two CERN[18] points at small angles. This figure indicates that at $\tilde{E} = 1191$ MeV, we are lower than most other experiments. We cannot offer a reasonable explanation for this. Because our "CEX-dependent" cross sections, based on the CEX/REX ratios given in Table IV, agree with our direct measure-

TABLE IV. Measured values of the CEX/REX ratio in our experiment. In the first column are listed the incident beam momentum in MeV/c and $\tilde{\theta}_\gamma$ in degrees for each data point. The third column gives the CERN phase-shift prediction (see Ref. 10) for CEX. The last column is our "indirect" REX measurement and is obtained by dividing the CERN phase-shift CEX value by the CEX/REX ratio and the detailed-balance factor.

Data point p_π-$\tilde{\theta}_\gamma$	P	CEX (mb/sr)	$\gamma n \to \pi^- p$ (μb/sr)
239-80	32.2 ± 2.3	1.55	16.8 ± 1.2
239-100	32.1 ± 3.1	1.82	19.8 ± 1.9
239-120	51.5 ± 4.6	3.15	21.3 ± 1.9
239-140	81.6 ± 9.7	5.13	21.9 ± 2.6
264-70	46.8 ± 3.4	2.75	21.6 ± 1.6
264-90	26.9 ± 2.2	2.00	27.3 ± 2.3
264-110	39.1 ± 5.0	2.65	24.8 ± 3.2
264-130	63.4 ± 8.4	4.45	25.8 ± 3.4
264-142	70.8 ± 10.2	5.66	29.4 ± 4.2
295-70	87.4 ± 12.3	3.21	14.2 ± 1.7
295-90	45.2 ± 6.4	2.07	17.7 ± 2.4
295-110	40.8 ± 4.9	2.39	22.6 ± 2.6
295-130	63.8 ± 10.8	3.91	23.7 ± 3.7
295-148	106 ± 20	5.59	20.3 ± 3.4
323-69	84.7 ± 11.7	3.02	14.3 ± 1.9
323-89	44.8 ± 6.8	1.71	15.2 ± 2.2
323-109	37.7 ± 5.0	1.64	17.4 ± 2.2
323-129	61.7 ± 10.3	2.60	16.9 ± 2.7
323-146	83.4 ± 12.4	3.75	18.0 ± 2.6
375-49	125 ± 14	3.98	13.4 ± 1.5
375-69	82.7 ± 9.1	2.22	11.3 ± 1.2
375-88	37.4 ± 3.1	1.03	11.6 ± 0.9
375-109	26.8 ± 2.5	0.69	10.8 ± 1.0
375-129	40.4 ± 6.9	1.02	10.6 ± 1.8
375-147	60.9 ± 6.8	1.52	10.4 ± 1.1

TABLE V. Final results of our experiment on $\pi^- p \to \gamma n$, expressed as $\gamma n \to \pi^- p$. D. B. = detailed-balance factor. In the second column are given the beam momentum and $\tilde{\theta}_\gamma$ of each data point as listed for reference in Tables III and IV.

	Data point p_{π^-}-$\tilde{\theta}_\gamma$	$\tilde{\theta}_{\gamma\pi^-}$ (deg)	$\cos\theta_\gamma$ -	$\gamma n \to \pi^- p$ $d\sigma/d\tilde{\Omega}$ (μb/sr)
$\tilde{E}$ = 1191 ± 2 MeV	239-60	60.4 ± 5.1	0.49 ± 0.08	13.7 ± 1.5
$p(\pi^-)$ = 239 MeV/c	239-80	79.7 ± 5.0	0.18 ± 0.08	17.4 ± 1.6
[$E(\gamma)$ = 285 MeV]	239-100	99.7 ± 5.3	−0.17 ± 0.09	20.2 ± 2.3
D. B. = 2.87	239-120	119.8 ± 5.5	−0.50 ± 0.08	21.4 ± 2.4
	239-140	140.2 ± 5.6	−0.77 ± 0.06	21.3 ± 2.8
$\tilde{E}$ = 1208 ± 2 MeV	264-56	56.0 ± 5.1	0.56 ± 0.07	16.4 ± 1.6
$p(\pi^-)$ = 264 MeV/c	264-70	70.3 ± 4.9	0.34 ± 0.08	21.8 ± 2.1
[$E(\gamma)$ = 307 MeV]	264-90	90.4 ± 5.3	−0.01 ± 0.09	27.7 ± 2.8
D. B. = 2.72	264-110	110.4 ± 5.5	−0.35 ± 0.09	26.5 ± 3.9
	264-130	130.4 ± 5.6	−0.65 ± 0.07	25.3 ± 3.6
	264-142	141.5 ± 5.7	−0.78 ± 0.06	29.4 ± 4.6
$\tilde{E}$ = 1230 ± 2 MeV	295-50	50.4 ± 4.4	0.64 ± 0.06	14.6 ± 2.2
$p(\pi^-)$ = 295 MeV/c	295-70	70.4 ± 5.0	0.34 ± 0.08	14.6 ± 2.1
[$E(\gamma)$ = 335 MeV]	295-90	90.4 ± 5.4	−0.01 ± 0.09	18.3 ± 2.8
D. B. = 2.59	295-110	110.4 ± 5.6	−0.35 ± 0.09	22.8 ± 3.0
	295-130	130.3 ± 5.7	−0.65 ± 0.08	23.2 ± 4.0
	295-148	148.0 ± 5.8	−0.85 ± 0.05	19.3 ± 3.4
$\tilde{E}$ = 1249 ± 2 MeV	323-69	69.3 ± 5.1	0.35 ± 0.08	14.5 ± 2.1
$p(\pi^-)$ = 323 MeV/c	323-89	89.3 ± 5.4	0.01 ± 0.09	15.2 ± 2.4
[$E(\gamma)$ = 360 MeV]	323-109	109.1 ± 5.6	−0.33 ± 0.09	17.3 ± 2.4
D. B. = 2.50	323-129	129.1 ± 5.8	−0.63 ± 0.08	15.8 ± 2.7
	323-146	146.2 ± 5.8	−0.83 ± 0.06	18.0 ± 2.8
$\tilde{E}$ = 1285 ± 3 MeV	375-49	49.1 ± 5.4	0.65 ± 0.07	13.6 ± 1.9
$p(\pi^-)$ = 375 MeV/c	375-69	68.6 ± 5.2	0.36 ± 0.08	11.3 ± 1.5
[$E(\gamma)$ = 409 MeV]	375-88	88.4 ± 5.6	0.03 ± 0.10	11.8 ± 1.3
D. B. = 2.38	375-109	108.5 ± 5.7	−0.32 ± 0.10	10.6 ± 1.2
	375-129	128.8 ± 5.8	−0.63 ± 0.08	10.4 ± 1.9
	375-147	146.7 ± 6.0	−0.84 ± 0.06	11.0 ± 1.6

ment given in Table III, we doubt that the reason would be an error in the beam contamination or one of the normalization factors.

In Ref. 1 we stressed the fact that a quantitative comparison of different experiments of cross sections that vary rapidly with energy must involve evaluating the error introduced by the uncertainty in the beam energy, and we called it the comparison error. In the present experiment the beam energy is better known than in our first experiment, and the comparison error is less important. Furthermore, in the present experiment we measure the cross sections at five energies across the resonance. Any systematic errors in the beam energy in our experiment or in the inverse would reveal itself as a shift of the peak in the total cross section. Figure 7 shows the total cross section for $\gamma n \to \pi^- p$ of this and various other experiments.[11,12,15,16,19]

For the quantitative comparison of our results with the inverse reaction, we employ the two methods outlined in our earlier paper.[1] The first method, which is model independent, is based on fitting the same Moravcsik expression both to our data and to the data from the inverse reaction.

The second method is based on a comparison of our results with the inverse reaction in terms of the Christ-Lee–Donnachie-Shaw[2,20] model. The results of this model-dependent test of time-reversal invariance will be discussed in Sec. V E.

The specific form of the Moravcsik fit used in the model-independent test is

$$\frac{d\sigma}{d\Omega}(x)=\frac{d\sigma}{d\Omega}(x)\Big|_{\text{Born}}+a_1\frac{(1-x^2)x}{1-\beta_\pi x}\frac{1}{1+\beta_N x}+\sum_{n=2}^{4}a_n x^{n-2}\,, \tag{7}$$

where $x=\cos\tilde{\theta}_{\pi\gamma}$ and $d\sigma(x)/d\Omega\,|_{\text{Born}}$ = electric part of the Born approximation, given in Ref. 1, and β_N, β_π = nucleon and pion velocity. Figure 8 gives the coefficients a_i vs the c.m. energy.

The total cross sections given in Fig. 7 are obtained from an integration of the Moravcsik-type fits. We have included in the fit to our data the two forward points given in the $\pi^-p\to\gamma n$ experiment of Schinzel *et al.*[18] at CERN, interpolated to our energies. Only at our lowest energy do we find a two-standard-deviation difference between our total cross section and the interpolated Tokyo, Bonn, and ABHHM results, with a similar discrepancy in the a_2 and a_4 coefficient. We note that also the PRFN data show lower total cross sections below the P_{33} resonance peak. At all other energies the total cross sections agree with the inverse reaction within the accuracy of about $\pm 10\%$.

Though only the statistical errors are included in the fit, the large errors in the coefficients prevent a meaningful model-independent test at this time. No systematic difference in energy dependence is observed. Using the coefficients to interpolate the data from the inverse reaction to our energies and angles, we calculate the minimum χ^2 for other data sets compared with ours. For the new Orsay data,[17] which are limited to backward angles, we interpolate our data to their energies and angles. Listed in Table VI are the χ^2 values obtained. We quote also the results when an overall systematic error of $\pm$ 10% in the experiments is included. Comparing with Tokyo and Bonn, we find that the χ^2/n_D (n_D = number of data points) is always less than 1 with the exception of the lowest energy point. Even this disagreement can be removed by a 10% change in relative normalization. The dip in backward direction found in the Orsay measurements is not substantiated by our results, and we find consequently χ^2/n_D greater than 1.

We conclude from the above that detailed balance is valid in the reaction $\pi^-p\rightleftarrows\gamma n$ in the energy region of the $P_{33}(1232)$ resonance. The foregoing analysis is made under the assumption that the impulse approximation can be applied in extracting $\gamma n\to\pi^-p$ cross sections from photoproduction experiments on a deuterium target. *We exclude the unlikely possibility that at all five energies*—before, on the peak, and after the P_{33} resonance—a possible time-reversal violation is just compensated by the breakdown in the impulse approximation. Thus, the experimentally observed validity

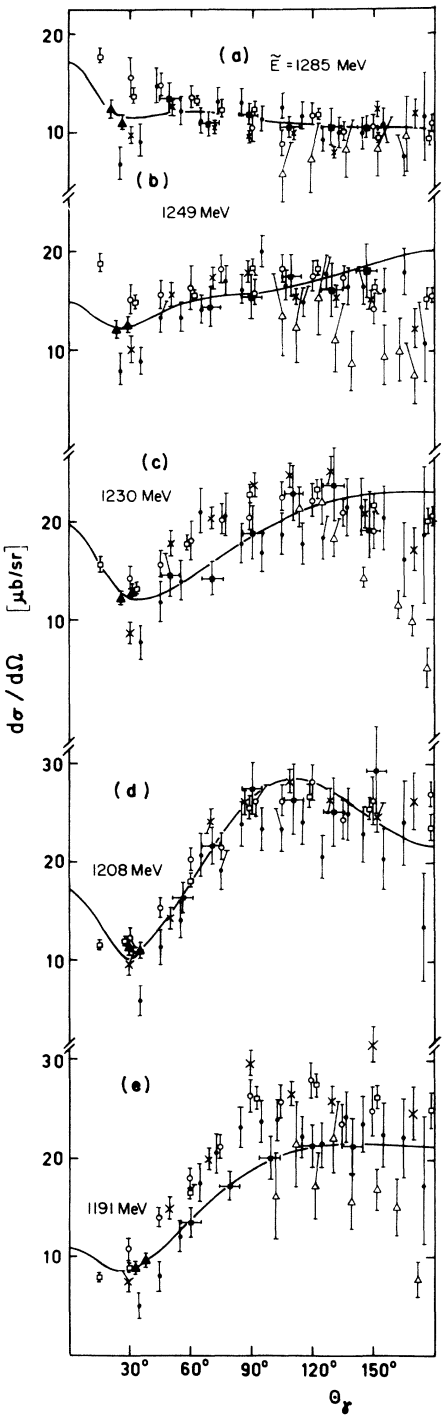

FIG. 6. Differential cross sections for $\gamma n\to\pi^-p$. Comparison of the data from this experiment with γd measurements interpolated to our energy. Solid curve is a Moravcsik fit to our data plus two points from Ref. 18. □ Bonn (see Ref. 11); ○ Tokyo (see Ref. 12); × ABHHM (see Ref. 15); ● PRFN (see Ref. 16); △ Boucrot *et al.* (see Ref. 17); ▲ CERN (see Ref. 18); ■ this experiment.

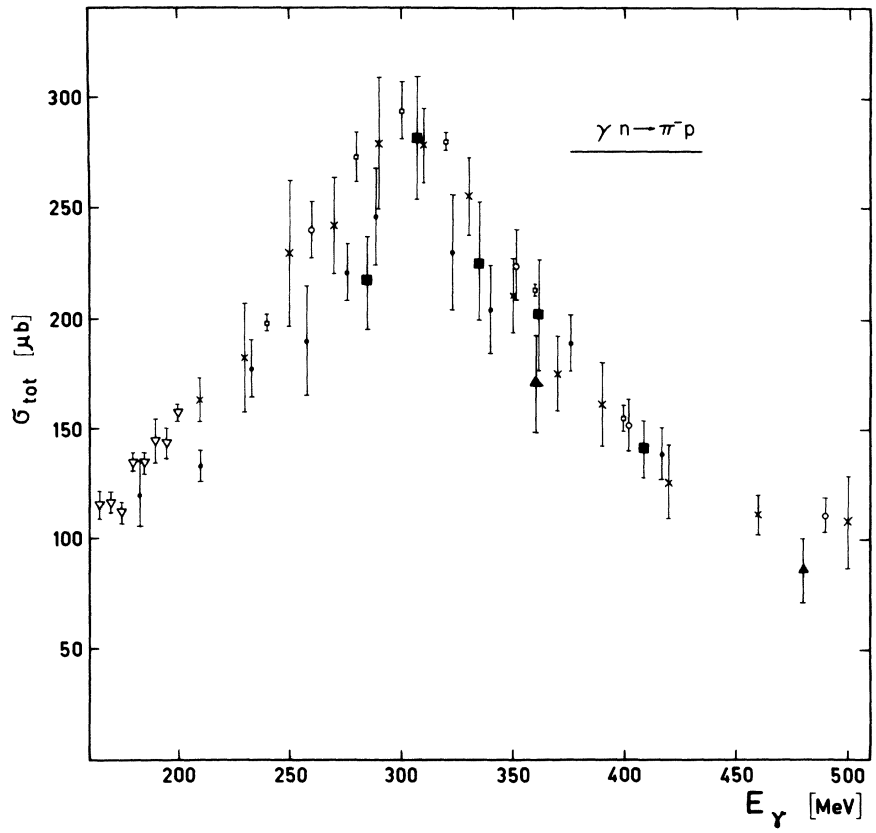

FIG. 7. Total cross sections for $\gamma n \rightarrow \pi^- p$ obtained from the integration of the Moravcsik fits. □ Bonn (see Ref. 11); ○ Tokyo (see Ref. 12); × ABHHM (see Ref. 15); ● PRFN (see Ref. 16); ▲ Berardo *et al.* (see Ref. 1); ▽ Adamovitch *et al.* (see Ref. 19); ■ this experiment.

of detailed balance indicates the validity of time-reversal invariance and the impulse approximation in the region of the P_{33}, within the experimental limits of 10–15%.

B. Comparison with other $\pi^- p \rightarrow \gamma n$ experiments

The Lausanne-Munich (L-M) collaboration[9] at CERN has measured REX at 60°, 90°, 120° using counter techniques. They rely heavily on the measurement of the neutron TOF to separate REX from CEX and accidentals. Their latest results are shown in Fig. 9 together with our data. After interpolating our results to the energies and angles of the L-M data, we can calculate the minimum χ^2 for the two data sets as described above. We find that χ^2/n_D is 2.8, 1.8, 0.5 for the 60°, 90°, 120° data sets, respectively. The agreement between the two experiments at 90° and 120° is acceptable, certainly when one considers that the experiments have several nontrivial difficulties such as the absolute calibration of the neutron-counter efficiency and the event extraction from a very large background. The reason that the agreement at 60° is so poor is unknown.

The results of our first experiment[1] are compared with the present experiment at $\tilde{E} = 1249$ MeV in Fig. 10. Some comments are in order. In the course of the analysis of the present data, we found a small correction to the result at $\tilde{E} = 1245$ MeV of our first experiment. The momentum of the 317 ± 6 MeV/c beam in that experiment was determined mainly by a range measurement, but no correction was applied for the range straggling. The necessary correction raises the beam momentum to 322 MeV/c with $\tilde{E} = 1248$ MeV. (There is no change in the other two beam momenta of our first experiment.) The agreement in the backward direction between the present experiment and our first one is marginal. The main difference between the two experiments was the set of π^0 anticounters around the hydrogen target to

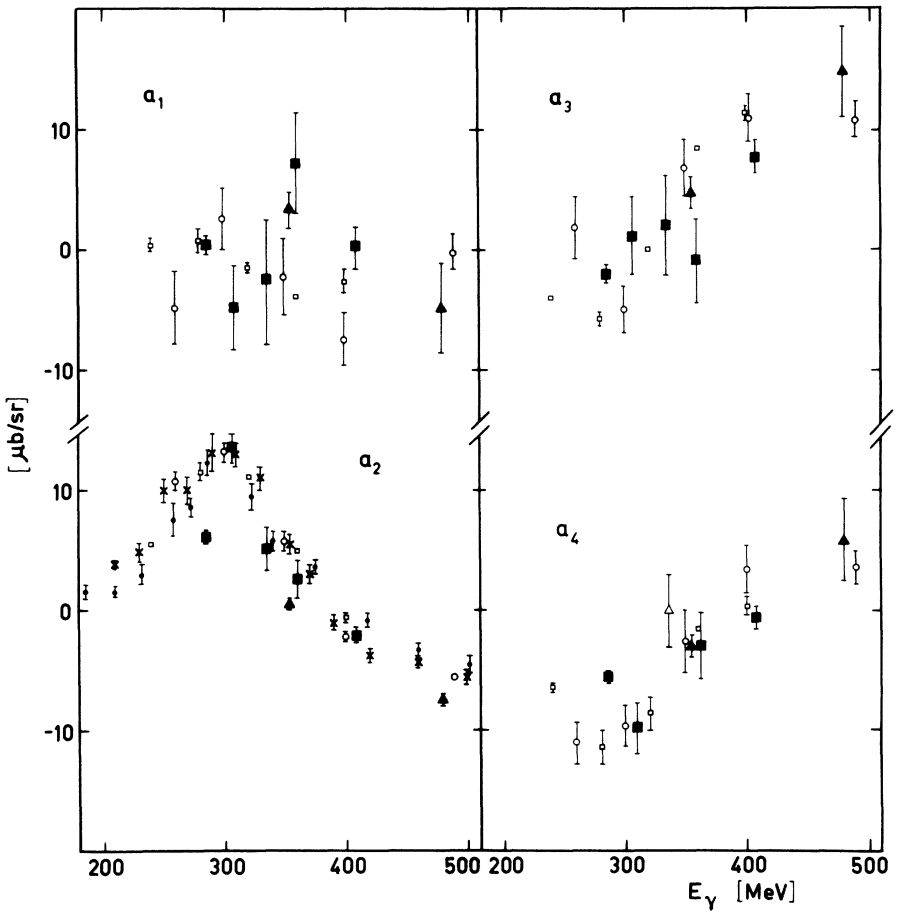

FIG. 8. Coefficients of the Moravcsik fit to $\gamma n \to \pi^- p$ differential cross sections. Symbols are the same as in Fig. 7. For the bubble chamber data, only a_2 is shown; the other coefficients have been omitted because they are essentially undetermined due to the large error in the data.

reduce triggering on CEX, and this set was not used in the present experiment. Also, the beam contamination of the present experiment is somewhat higher.

C. Test of the $|\Delta I| \leq 1$ rule

Sanda and Shaw[21] have introduced the "isotensor dip test" to investigate the possible existence of a $|\Delta I| = 2$ component of the electromagnetic interaction of hadrons. This test consists of determining $\Delta(\sigma)$, where

$$\Delta(\sigma) = \frac{k}{q} \left[\sigma_t(\gamma p \to \pi^- n) - \sigma_t(\gamma n \to \pi^+ p)\right],$$

k is the photon momentum, and q is the pion momentum. A dip in $\Delta(\sigma)$ in the region of the $P_{33}(1232)$ is the predicted manifestation of an isotensor component. Table VII shows $\Delta(\sigma)$ calculated from our total cross section for $\gamma n \to \pi^- p$ and the Bonn[13] and Orsay[14] measurements of $\gamma p \to \pi^+ n$. The large errors preclude drawing a meaningful quantitative conclusion. Our data are consistent with the 3% upper limit of the isotensor component recently deduced by Donnachie and Shaw[22] from the π^-/π^+ ratio measurements,[12] which are more suitable for the isotensor dip test, provided the charge-dependent corrections to the π^-/π^+ ratio have been properly assessed. Our results for $\Delta(\sigma)$ are in general smaller than the values obtained by Pfeil *et al.*[23] and by Suzuki *et al.*,[24] who performed a conventional multipole analysis of the Bonn π^+ and π^- data[11,14] supplemented by the 180° Tokyo results[12] without using exotic currents. In a conventional analysis,[25] $\Delta(\sigma)$ is an indication of the isoscalar contribution in photoproduction. Therefore our isoscalar contribution is less than that of the above authors. See also Sec. V D.

TABLE VI. Comparison of $\gamma n \to \pi^- p$ obtained via detailed balance from our $\pi^- p \to \gamma n$ experiment with $\gamma n \to \pi^- p$ derived from recent γd experiments. Interpolations are based on a linear interpolation of the coefficients of Eq. (7), that was used to fit the data. The last column gives the χ^2 per data point calculated using the statistical errors only. The next to last column gives the χ^2 per data point when an additional systematic 10% error in relative normalization is included.

$\gamma n \to \pi^- p$ from γd	Energy of data set in MeV	Number of data points	χ^2/n_D Statistical error + normalization error	χ^2/n_D Statistical error
PRFN (Ref. 16)	1191	5	0.72	1.29
	1208	6	0.65	0.85
	1230	6	0.35	0.42
	1249	6	0.17	0.23
	1285	6	0.27	0.38
ABHHM (Ref. 15)	1191	5	1.14	1.75
	1208	6	0.16	0.22
	1230	6	0.60	0.37
	1249	6	0.50	0.60
	1285	6	0.25	0.33
Tokyo (Ref. 12)	1191	5	1.67	3.28
	1208	6	0.25	0.37
	1230	6	0.44	0.62
	1249	6	0.23	0.29
	1285	6	0.35	0.47
Bonn (Ref. 11)	1191	5	2.19	4.82
	1208	6	0.27	0.41
	1230	6	0.10	1.22
	1249	6	0.36	0.53
Orsay (Ref. 17)	1191	10	5.10	
	1223	9	2.91	
	1253	10	1.96	
	1281	6	1.16	

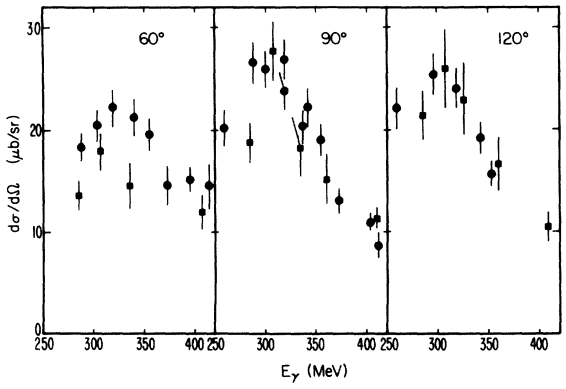

FIG. 9. Comparison of our results on $\gamma n \to \pi^- p$, obtained via detailed balance from $\pi^- p \to \gamma n$, with the data from Lausanne-Munich. ● Lausanne-Munich (see Ref. 9); ■ this experiment.

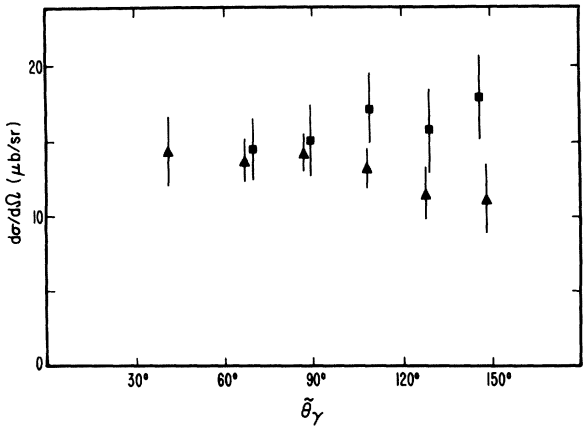

FIG. 10. Comparison of present experiment at $\tilde{E} = 1249$ MeV with our first experiment at $\tilde{E} = 1248$ MeV. ■ present experiment; ▲ Berardo *et al.* (see Ref. 1).

TABLE VII. Isotensor dip test.

$\tilde{E}$ (MeV)	$\sigma_t(\gamma n \to \pi^- p)$ (μb) UCLA [a]	$\sigma_t(\gamma p \to \pi^+ n)$ (μb) Bonn [b]	Orsay [c]	$\Delta(\sigma) = \frac{k}{q}[\sigma_t(\pi^-) - \sigma_t(\pi^+)]$ (μb) UCLA-Bonn	UCLA-Orsay
1191	216 ± 23	218 ± 13		−2 ± 31	
1208	284 ± 29	235 ± 14		57 ± 37	
1230	226 ± 26	215 ± 13	202 ± 8	13 ± 23	27 ± 29
1249	195 ± 24	176 ± 11	164 ± 7	21 ± 29	35 ± 28
1285	143 ± 14	118 ± 7	110 ± 5	27 ± 17	36 ± 16

[a] From $\pi^- p \to \gamma n$, this experiment.
[b] Fischer *et al.* (Ref. 14).
[c] Betourne *et al.* (Ref. 13).

D. Multipole analyses

The various published multipole analyses[23-32] of pion photoproduction, with the exception of the parameter-free dispersion-relation calculation of Berends *et al.*,[25] contain some adjustable parameters. The authors determine these adjustable parameters from a fit to the photoproduction data existing at the time of writing, and they include $\gamma n \to \pi^- p$ data obtained from measurements with a deuterium target. Therefore, the agreement or disagreement of our data with the multipole analyses reflects the consistency of our data with the data used in the specific analysis.

In the analysis of the region $\tilde{E} < 1300$ MeV, only s waves and p waves are considered, and only a limited number of multipole amplitudes are actually determined from experiment, namely the electric dipole E_{0+}, magnetic dipoles M_{1+} and M_{1-}, and the electric dipole E_{1+} amplitudes. The higher partial waves are evaluated from theory. It is assumed in all analyses that the phases of the multipoles are given via the Watson theorem[33] by their πN scattering phase-shift values.

Listed in Table VIII are all relevant multipole analyses,[23-32] except the one that includes exotic currents[20] and which will be discussed in Sec. V E, the input data,[11,12,15,16,33-36] and the assumptions used in each. In Fig. 11 we show the results of all the analyses that have published angular distributions or multipole values, interpolated to our energies. Shown in Fig. 12 are the values for the real part of the s- and p-wave multipoles obtained by different authors for the $\pi^- p \to \gamma n$ channel. The following conclusions can be drawn from the comparison of our data with the calculations.

(1) The multipole analyses based on fixed-t dispersion relations without adjustable parameters are not in agreement with our data. Berends *et al.*[25] predict values for the total cross section which are too large as well as differential cross sections that are enhanced in the backward direction. A similar behavior is predicted by the calculation of Ref. 26. The difference with our data can be reduced by a slight decrease in the E_{0+} and M_{1-} multipoles.[28]

(2) Schwela's calculations[27] are in better agreement with our results, although our data are somewhat lower at the low energies and somewhat higher at the high energies. Schwela makes an energy-dependent ansatz for E_{0+} and M_{1-} and his fits are based on the experimental data[36] pre-1968.

(3) Below the peak of the $P_{33}(1232)$ resonance, our data are in good agreement with the work of Ball *et al.*[29] Above the resonance the calculations are somewhat lower than the data, especially in the backward direction. The fixed-t dispersion-relation–type calculation by Ball *et al.* is done as follows. The photon-nucleon interaction is given by the Born terms and the strong final-state interactions, including inelastic reactions, are treated as a rescattering correction with a phenomenological parameterization. The parameters are determined from the data. It is found that the E_{0+} multipole, and to a lesser extent the M_{1+}, are influenced by the inelastic channels, even at low energies. The $E_{0+}(\pi^-)$ is quite different from the one in the above analyses. It would be interesting to update the calculation of Ball *et al.* using the most recent photoproduction data, especially in the π^- channel.

(4) The isobar model calculations agree quite well with our data. Walker[30] fits pre-1968 data[36] to a sum of resonances, Born terms, and a smoothly varying nonresonant background. Moorhouse *et al.*[31] evaluate the contribution of the isobar and the smooth background separately for the imaginary components, while the real part of the multipoles are calculated from dispersion integrals. The

TABLE VIII. Multipole analyses and theoretical calculations for pion photoproduction used in Figs. 11 and 12.

Name of calculation	Reference	π-N phases	Adjusted multipoles	$\gamma n \to \pi^- p$ data ref.	Higher multipoles
Fixed-t dispersion relations without adjustable parameters (single channel)	Berends *et al.*[25]				
	Engels *et al.*[26]	Roper *et al.*[a]			
		Auvil *et al.*[b]			
		Bareyre *et al.*[c]			
Fixed-t dispersion relations with adjustable parameters (single channel)	Schwela[27]		E_{0^+}, M_{1^-}	36	
	Berends *et al.*[28]		M_{1^-}		
Fixed-t dispersion relations with adjustable parameters (multichannel)	Ball *et al.*[29]			15, 16, 33	
Isobar model (resonances + Born + smooth nonresonant background)	Walker[30]		$l \leq 3$ energy dependent	36	Born
	Moorhouse *et al.*[31]		$l \leq 3$ energy dependent	34, 35, 15	Born
Multipole analysis — energy independent	Noelle *et al.*[32]	Particle Data UCRL-20030	$E_0, M_{1^-}, E_{1^+}, M_{1^+}$	15, 16, 34, 35, 36	Born
	Pfeil *et al.*[23]	Almehed *et al.*[10]	$E_0, M_{1^-}, E_{1^+}, M_{1^+}$	11, 34, 35, 36	Born
	Suzuki *et al.*[24]	Particle Data UCRL-20030	$E_0, M_{1^-}, E_{1^+}, M_{1^+}$ energy independent	11, 12, 34, 35	BDW, Ref. 25

[a] L. Roper *et al.*, Phys. Rev. 138, B190 (1965).
[b] P. Auvil *et al.*, Phys. Lett. 12, 76 (1964).
[c] P. Bareyre *et al.*, Phys. Lett. 18, 342 (1965).

values for E_{0^+} and M_{1^-} obtained are in reasonable agreement with the results of Schwela and Ball *et al.*

(5) The above multipole analyses substantially agree on the M_{1^+} and E_{1^+} contributions to the P_{33} resonances. Some minor differences are due to the choice of π-N phase shifts, recent versions of which have shifted the resonance position to lower energy. This is directly reflected in the value of the energy where M_{1^+} becomes zero. The recent energy-independent analyses by Suzuki *et al.*,[24] Noelle and Pfeil,[32] and Pfeil and Schwela[23] show an almost pure Breit-Wigner shape for the P_{33}. Pfeil and Schwela and Suzuki *et al.* obtain slightly different values for the E_{0^+} and M_{1^-} multipoles, although they use similar input data sets and the higher multipoles given by the Born approximation or by the Berends *et al.* calculation, which give similar values. The results agree within error bars below resonance, but not above. The effect this difference has on the cross section is very small, and our data cannot distinguish between the various multipole analyses. A planned experiment that uses a polarized proton target will be very important here.[37]

The solution of Noelle and Pfeil,[32] which is influenced by their preference for the PRFN[16] data and preliminary ABHHM results, is consistent with our data at $\bar{E} = 1208$ and 1285 MeV. These authors find a strong energy dependence of $\mathrm{Re}E_{0^+}$ and a smaller magnitude.

To investigate the influence of our new data on the isospin decomposition of the E_{0^+} and M_{1^-} multipoles, which are uncertain at present, we made a fit to our data using the Pfeil and Schwela (PS)[23] analysis but varied $E_{0^+}^{(1/2)}$ and $M_{1^-}^{(1/2)}$. This preserves the good PS fit to the π^+ photoproduction data. We used for $M_{1^+}(\pi^-)$ and $E_{1^+}(\pi^-)$ the PS values except at $\bar{E} = 1191$ MeV, where M_{1^+} was varied also. We find that on the average $E_{0^+}^{(1/2)}(\pi^-)$ is reduced by 19% compared to PS. Using $E_{0^+}^{(1/2)}(\pi^+)$ from PS, this amounts to an average reduction of $E_{0^+}^{(1)}$ by 9% and makes $E_{0^+}^{(0)}$ consistent with zero at all our energies. Similarly, we find a decrease of

23% in $M_{1-}(\pi^-)$ corresponding to a 21% increase of $M_{1+}^{(1)}$ and a sizable energy dependence of $M_{1-}^{(0)}$. We give the values for $\mathrm{Re}E_{0+}(\pi^-)$ and $\mathrm{Re}M_{1-}(\pi^-)$ in Fig. 12; the error bars are omitted since they are not meaningful, because we did not perform a full-scale PS-type analysis of all $\pi^- p \to \gamma n$ results.

E. Test of time-reversal invariance in the Christ-Lee–Donnachie-Shaw model

In the Christ-Lee model[2] as applied by Donnachie and Shaw,[20] the T-violating phases are considered only in the isovector and presumed isotensor part of the dominant $M_{1+}^{(3/2)}$ multipole. The parameterization used by Donnachie and Shaw is

$$
\begin{aligned}
{}_pM_{1+}^{(3/2)} &= (\tfrac{2}{3})^{1/2} M(W)[x_2 \exp(ix_4) - (\tfrac{3}{5})^{1/2} x_3 \exp(ix_5)] \\
&= (\tfrac{2}{3})^{1/2} M(W) x_p \exp(i\phi_p) , \\
{}_nM_{1+}^{(3/2)} &= (\tfrac{2}{3})^{1/2} M(W)[x_2 \exp(ix_4) + (\tfrac{3}{5})^{1/2} x_3 \exp(ix_5)] \\
&= (\tfrac{2}{3})^{1/2} M(W) x_n \exp(i\phi_n) ,
\end{aligned}
$$

with

$$
M(W) = \frac{Ak}{q^2} \exp(i\delta_{33}) \sin\left(\delta_{33} + x_4 \frac{q^3}{k^3}\right) .
$$

The variables are defined in Ref. 20. The T-violating phases x_4 and x_5 change sign under time reversal. When $x_4 = x_5 = 0$ one finds $x_2 M(W) = -\frac{1}{3} A^{(V)}$ and $x_3 M(W) = -\frac{1}{3} A^{(T)}$, where $A^{(V)}$ and $A^{(T)}$ are the familiar isovector and isotensor parts of the $I = \frac{3}{2}$ amplitude.

A quantitative test of time-reversal invariance using the above Christ-Lee–Donnachie-Shaw model was done as follows. First we performed a conventional multipole fit to our own data augmented by the forward data points of CERN.[18] A similar fit was made to the inverse reaction, for which we chose the Bonn[11] and Tokyo[12] data interpolated to our energies. In the fits we used the phenomenological multipoles of Pfeil and Schwela[21] since they fit the $\gamma p \to \pi^0 p$ and $\gamma n \to \pi^0 n$ data, modifying only the $E_{0+}(\pi^-)$ and $M_{1-}(\pi^-)$ multipoles. Since the isotensor component is zero or small, Donnachie and Shaw quote $x_3/x_2 < 0.03$ (see Sec. V C), we limited the analysis to the case $x_3 = 0$ and $x_2 = 1 = x_n = x_p$ and $\phi_p = \phi_n = x_4$. In other words, the T violation is restricted to the isovector part of $M_{1+}^{(3/2)}$ only. Finally, we made a simultaneous fit to our data and the inverse using the average of the multipole values obtained above from the independent fit to our data and to the inverse reaction, only varying the T-violating phase of $M_{1+}^{(3/2)}$. The results for each of our five energies are given in Table IX. The average value of the T-violating phase $\phi_n = -1.1° \pm 0.8°$ is consistent with zero and no violation of time-reversal invariance. A safe upper limit for ϕ is 2°, which is a substan-

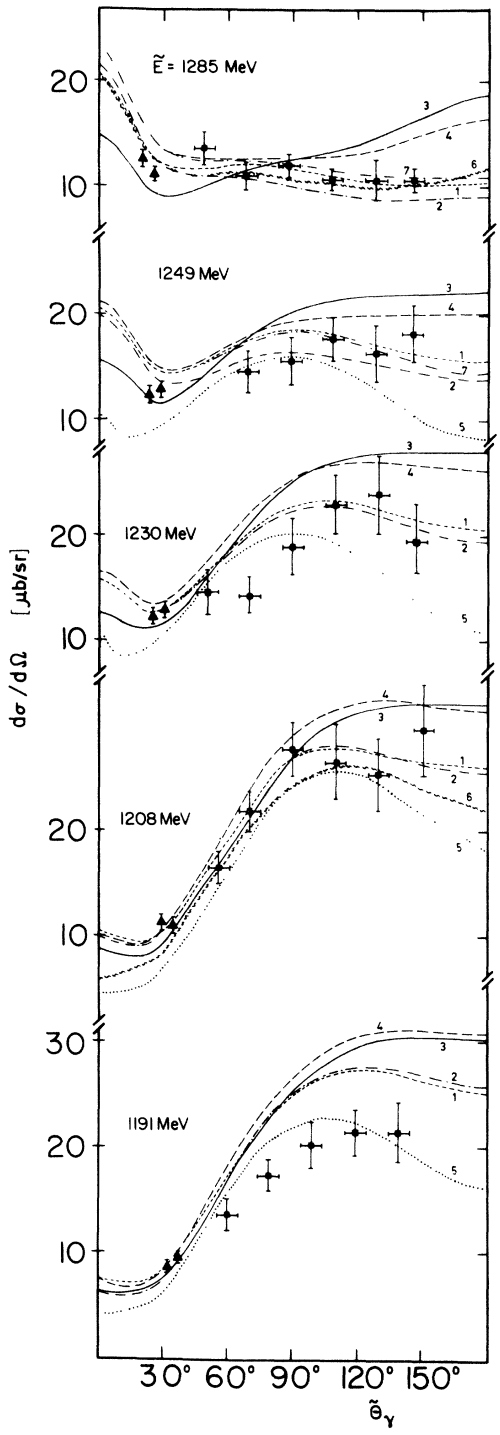

FIG. 11. Multipole analyses and theoretical predictions compared with the data from this experiment (■) and those from Ref. 18 (▲). (1) Pfeil, Schwela (see Ref. 23); (2) Schwela (see Ref. 27); (3) Berends, Donnachie, Weaver (see Ref. 25); (4) Schmidt (see Ref. 26); (5) Ball, Campbell, Shaw (see Ref. 29); (6) Noelle, Pfeil (see Ref. 32) (E_γ = 300 and 420 MeV); (7) Suzuki, Kurokawa, Kondo (see Ref. 24).

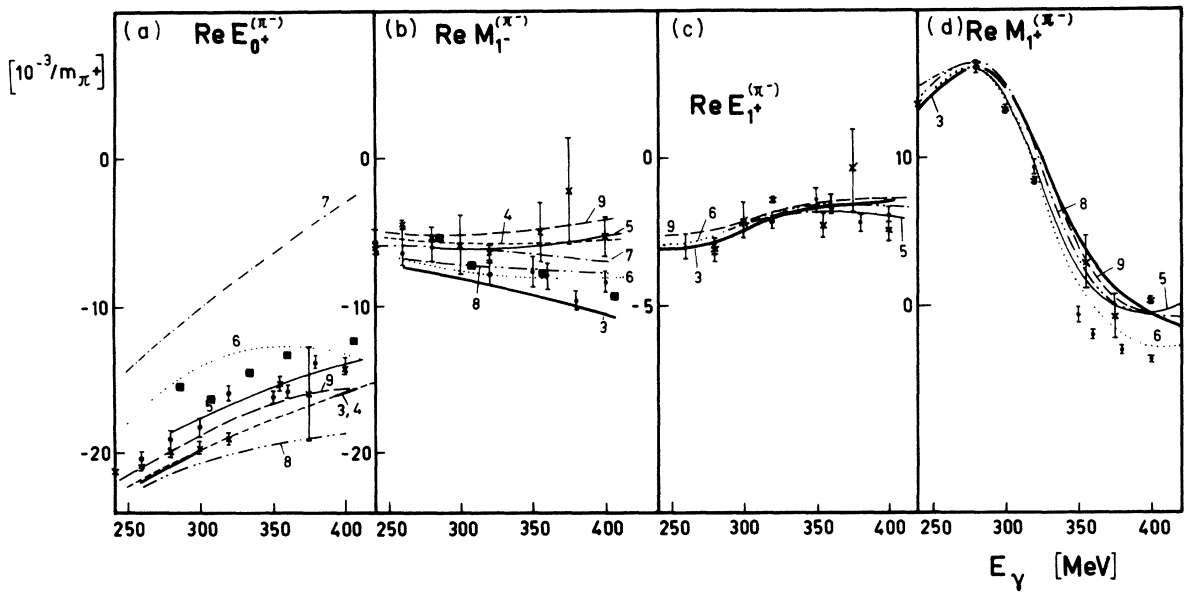

FIG. 12. Results of various multipole analyses and theoretical predictions for the real parts of the leading s- and p-wave multipoles for π^- photoproduction: ● Pfeil, Schwela (see Ref. 23); ×Suzuki, Kurokawa, Kondo (see Ref. 24); (3) Berends, Donnachie, Weaver (see Ref. 25); (4) Moorhouse, Oberlack, Rosenfeld (see Ref. 31); (5) Schwela (see Ref. 27); (6) Noelle, Pfeil (see Ref. 32); (7) Ball, Campbell, Shaw (see Ref. 29); (8) Schmidt (see Ref. 26); (9) Walker (see Ref. 30); ■ fit to our data points.

tial improvement over the result of related experiments.[38-40]

Shown in Fig. 13 are the fit to our data and some selected results of the inverse reaction, plus the effect of a $\pm 6^\circ$ T-violating phase in $M_{1+}^{(3/2)}$ calculated in the manner just outlined. Though at some points there seems to be a small difference between $\gamma n \to \pi^- p$ and the inverse reaction, if one insists on consistency among the results of our five beam energies in the spirit of the Christ-Lee-Donnachie-Shaw model, there is no evidence that detailed balance is not valid.

F. CEX/REX ratio

The CEX/REX ratio is measured at a particular angle in the laboratory and it is not a covariant quantity. The Jacobians for CEX and REX at the five energies of this experiment are not very different; therefore we may regard the substantial variations in the CEX/REX ratio to be representative of the relative variation in the center of mass of REX compared to CEX. The CEX/REX ratios measured in this experiment are given in Table IV. They are also shown in Fig. 14 vs $\langle\cos\tilde{\theta}\rangle \equiv \frac{1}{2}(\cos\tilde{\theta}_{\pi^0} + \cos\tilde{\theta}_\gamma)$. The energy of the CEX neutrons near $\cos\tilde{\theta} = 0.7$ of the four lowest energies is too low for us to make reliable CEX measurement, although the REX is easily measurable. For these four points we have obtained the CEX/REX ratios by dividing the CERN CEX value by our measured REX result.

Figure 14 shows that the angular variation of the CEX/REX ratios in our energy region is considerable and has a typical bowl shape. The reason that the CEX/REX ratio has this shape is the following. The CEX cross section is dominated by the $P_{33}(1232)$ resonance. In the vicinity of the peak of this resonance, the angular distribution has the characteristic $(1 + 3\cos^2\theta)$ shape of a p-

TABLE IX. Numerical results of a test of time-reversal invariance in the Christ-Lee–Donnachie-Shaw model. Our data augmented by 2 forward points of CERN (see Ref. 18) are compared with those of Bonn (see Ref. 11) and Tokyo (see Ref. 12) assuming that the difference is due to a T-violating phase ϕ in the $M_{1+}^{(3/2)}$ multipole. The third column shows the χ^2 per degree of freedom for the comparison.

$\tilde{E}$ (MeV)	ϕ (deg)	χ^2/n	Number of data points $\pi^- p \to \gamma n$	$\gamma n \to \pi^- p$
1191	1.1 ± 3.2	3.9	7	16
1208	-3.4 ± 1.1	0.6	8	17
1230	0.4 ± 1.4	1.1	8	17
1249	-2.0 ± 1.9	1.6	7	17
1285	-2.3 ± 2.5	1.9	8	17
Average	-1.1 ± 0.8	1.8		

wave resonance. The REX cross section is dominated also by the P_{33} but its radiative decay proceeds via the magnetic dipole transition which has a $(2+3\sin^2\theta)$ angular distribution. Figure 14 shows in a qualitative way that the decay of the P_{33} via the electric quadrupole transition, which has a $(1+\cos^2\theta)$ dependence, is suppressed. This suppression appears in all multipole analyses,[23-32] and it is one of several remarkable predictions that were made when the quark model was applied in calculating[41] the radiative decay of various resonances.

VI. CONCLUSION

Our measurements of the differential cross section for $\pi^-p\to\gamma n$ around the $P_{33}(1232)$ resonance are in agreement with most of the data on the inverse reaction, Fig. 6 and Table VII. Because of the sensitivity for testing the validity of detailed balance in $\pi^-p\to\gamma n$ at our energies, as discussed for example by Christ and Lee,[2] our results provide a good test of the validity of time-reversal invariance in the electromagnetic interaction of hadrons (see Fig. 13 and Table IX). We can place an upper limit of 2° to a possible T-violating phase of the isovector component of the electromagnetic current.

It is worthwhile to point out that the demonstrated validity of detailed balance here implies that the impulse approximation is good to about 15% for extracting γn data from γd experiments even in the region of the strong $P_{33}(1232)$ resonance.

Our new data show the limited usefulness of the known multipole analyses for π^- photoproduction. Figure 11 illustrates the fact that none of the published multipole evaluations are capable of fitting all our new data.

Finally, our experiment is consistent with the traditional decomposition of the electromagnetic current in only isoscalar and isovector components, without isotensor.

ACKNOWLEDGMENTS

We gratefully acknowledge the loan of the Vidicon system by Professor V. Perez-Mendez of LBL, the help of Mr. M. Arman and Mr. R. Belisle with the setting up of the experiment, and the help of Mr. G. Fucik, Mr. S. White, and Mr. R. Danao with the analysis. We appreciate the interest shown by Professor K. Crowe, and we thank Mr. J. Vale and the cyclotron crew for their dedicated efforts.

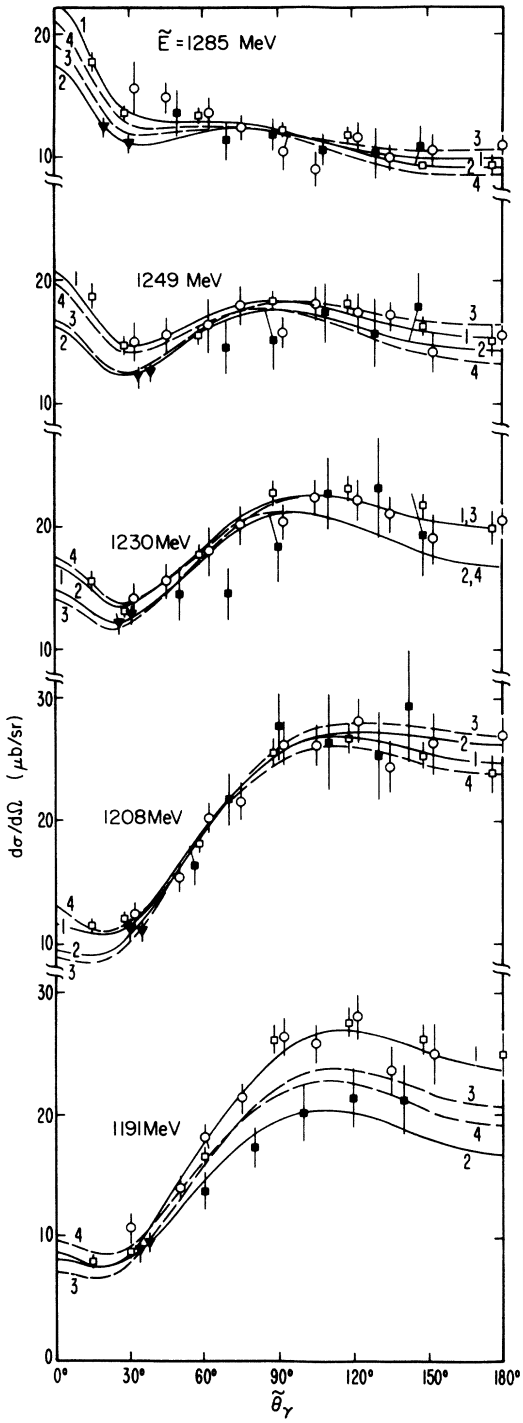

FIG. 13. Test of time-reversal invariance in $\gamma n \rightleftarrows \pi^-p$ based on the Christ-Lee–Donnachie-Shaw model. Curve 1: Conventional multipole fit to $\gamma n\to\pi^-p$ data. Curve 2: Conventional multipole fit to our $\pi^-p\to\gamma n$ data, augmented by the CERN small angle data (see Ref. 18). Curve 3: Effect of a T-violating phase $\phi=-6°$ in the isovector part of $M_1{}^+$. Curve 4: Same as curve 3 but for $\phi=+6°$. Note that $\phi=0$ corresponds to the average of curves 1 and 2. ■ this experiment; ▼ CERN (see Ref. 18); □ Bonn (see Ref. 11); ○ Tokyo (see Ref. 12).

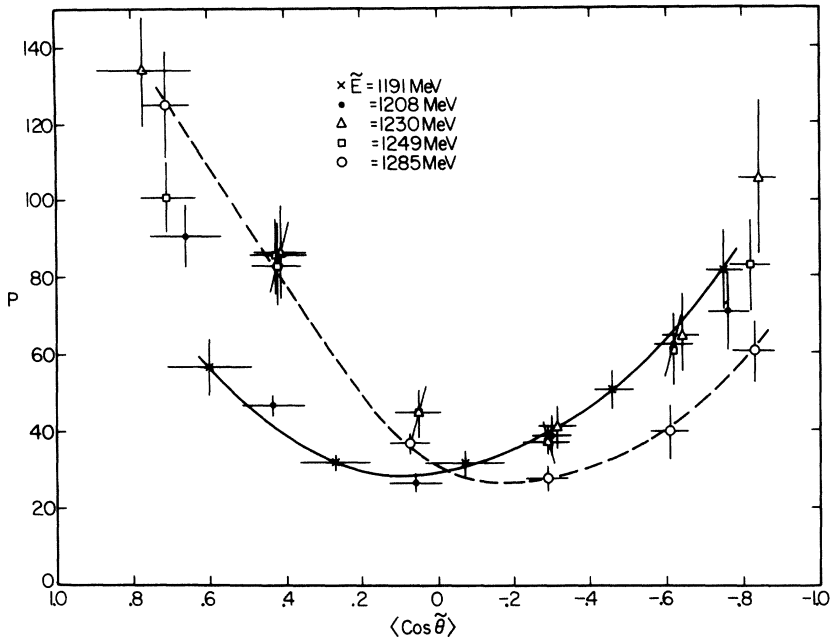

FIG. 14. Ratio $P = d\sigma(\pi^- p \to \pi^0 n)/d\sigma(\pi^- p \to \gamma n)$ as a function of $\langle \cos\tilde{\theta} \rangle = \frac{1}{2}(\cos\tilde{\theta}_{\pi^0} + \cos\tilde{\theta}_\gamma)$. The solid line is an eye-guiding line through the $\tilde{E} = 1191$ MeV data; the dashed line is through our $\tilde{E} = 1185$ MeV data.

---

*Work supported in part by the U. S. Atomic Energy Commission.

†Present address: Physics Dept., Univ. of Virginia, Charlottesville, Virginia 22901.

‡Present address: SUNY, Buffalo, New York 14222.

§Present address: Physik Institut der Universität Zürich, Zürich, Switzerland.

‖Present address: Physics Department, Harvard University, Cambridge, Massachusetts 02138.

[1]P. A. Berardo, R. P. Haddock, B. M. K. Nefkens, L. J. Verhey, M. E. Zeller, A. S. L. Parsons, and P. Truoel, Phys. Rev. D 9, 621 (1974).

[2]N. Christ and T. D. Lee, Phys. Rev. 148, 1520 (1966).

[3]A. S. L. Parsons *et al.*, Nucl. Instrum. Methods 79, 43 (1970).

[4]P. A. Berardo, UCLA Ph.D. thesis, 1970 (unpublished).

[5]J. C. Comiso, UCLA Ph.D. thesis, 1972 (unpublished).

[6]W. H. Barkas and M. J. Berger, NASA Report No. NASA SP-3013, 1964 (unpublished).

[7]J. C. Comiso *et al.*, following paper, Phys. Rev. D 12, 738 (1975).

[8]D. V. Bugg *et al.*, Nucl. Phys. B26, 588 (1971).

[9]L. H. Guex *et al.*, Phys. Lett. 55B, 101 (1975).

[10]Particle Data Group phase-shift tape, LBL, Berkeley, 1974 (unpublished); R. Kelly, private communication. CERN phases are listed as Almehed 72 [see S. Almehed and C. Lovelace, Rutgers Univ. report 1972 (unpublished)]. Saclay phases are the Saclay 1974 ones (K. Ayed, private communication to Particle Data Group). Carter phases are obtained directly from the listing in Carter *et al.*, Nucl. Phys. B58, 378 (1973).

[11]G. von Holtey *et al.*, International Symposium on Electron and Photon Interactions at High Energies, Bonn, 1973, contributed paper No. 52 (unpublished); preliminary results in Phys. Lett. 40B, 589 (1972).

[12]T. Fujii *et al.*, International Symposium on Electron and Photon Interactions at High Energies, Bonn, 1973, contributed paper No. 41 (unpublished); preliminary results in Phys. Rev. Lett. 28, 1672 (1972).

[13]C. Betourne *et al.*, Phys. Rev. 172, 1343 (1968).

[14]G. Fischer *et al.*, Z. Phys. 253, 38 (1972).

[15]Aachen-Bonn-Hamburg-Heidelberg-Munchen (ABHHM) Collaboration; P. Benz *et al.*, Nucl. Phys. B65, 158 (1973).

[16]Pavia-Roma-Frascati-Napoli (PRFN) Collaboration; V. Rossi *et al.*, Frascati Report LNF-72131, 1972 (unpublished). Preliminary results are given in Nuovo Cimento Lett. 3, 697 (1970); *ibid.* 2, 1183 (1971).

[17]J. Boucrot *et al.*, Nuovo Cimento 18, 635 (1973).

[18]D. Schinzel, thesis, Karlsruhe, 1971 (unpublished). Preliminary results are given in J. Favier *et al.*, Phys. Lett. 31B, 609 (1970).

[19]M. I. Adamovitch *et al.*, Yad. Fiz. 9, 848 (1969) [Sov. J. Nucl. Phys. 9, 496 (1969)].

[20]A. Donnachie and G. Shaw, Phys. Lett. B35, 419 (1971); also Phys. Rev. D 5, 1117 (1972).

[21]A. I. Sanda and G. Shaw, Phys. Rev. Lett. 24, 1310 (1970); Phys. Rev. D 3, 243 (1971); Phys. Rev. Lett. 26, 1053 (1971).

[22]A. Donnachie and G. Shaw, International Symposium on Electron and Photon Interactions at High Energies, Bonn, 1973, contributed paper No. 31 (unpublished).

[23]W. Pfeil and D. Schwela, Nucl. Phys. B45, 379 (1972).
[24]S. Suzuki, S. Kurokawa, K. Kondo, International Symposium on Electron and Photon Interactions at High Energies, Bonn, 1973, contributed paper No. 263 (unpublished).
[25]F. A. Berends, A. Donnachie, and D. L. Weaver, Nucl. Phys. B4, 1 (1968).
[26]J. Engels, A. Mullensiefen, and W. Schmidt, Phys. Rev. 175, 1951 (1968); W. Schmidt, private communication.
[27]D. Schwela, Z. Phys. 221, 158 (1969).
[28]F. A. Berends and A. Donnachie, Phys. Lett. 30B, 555 (1969); also A. Donnachie, Phys. Lett. 24B, 420 (1969).
[29]J. S. Ball, R. R. Campbell, and G. L. Shaw, Rev. D 8, 232 (1973).
[30]R. L. Walker, Phys. Rev. 182, 1729 (1969).
[31]R. G. Moorhouse, H. Oberlack, and A. H. Rosenfeld, Phys. Rev. D 9, 1 (1974).
[32]P. Noelle and W. Pfeil, Nucl. Phys. B31, 1 (1971).
[33]K. M. Watson, Phys. Rev. 95, 228 (1954).
[34]T. Fujii *et al.*, Phys. Rev. Lett. 26, 1672 (1971).
[35]K. Kondo *et al.*, J. Phys. Soc. Jpn. 29, 5102 (1970); also T. Nishikawa *et al.*, Phys. Rev. Lett. 21, 1288 (1968).
[36]Pre-1968 data: M. Beneventano *et al.*, Nuovo Cimento 10, 1109 (1958); M. Sands *et al.*, Phys. Rev. 95, 592 (1954); 96, 849 (1954); M. Bazin and J. Pine, Phys. Rev. 132, 2739 (1963); J. P. Burq and J. K. Walker, Phys. Rev. 132, 447 (1963); F. F. Liu *et al.*, Phys. Rev. 136, 1183 (1964).
[37]B. M. K. Nefkens *et al.*, LAMPF Proposal No. 58, 1972 (unpublished).
[38]S. Rock *et al.*, Phys. Rev. Lett. 24, 748 (1970).
[39]B. Schrock *et al.*, Phys. Rev. Lett. 26, 1659 (1971).
[40]D. Bartlett *et al.*, Phys. Rev. Lett. 27, 881 (1971).
[41]C. Becchi and G. Morpurgo, Phys. Rev. Lett. 17, 352 (1965).